The Plant Cell, Vol. 31: 486–501, February 2019, www.plantcell.org © 2019 ASPB.

The PROTEIN PHOSPHATASE4 Complex Promotes Transcription and Processing of Primary microRNAs in Arabidopsis

Suikang Wang,[a,b,c] Li Quan,[c,d] Shaofang Li,[c,e] Chenjiang You,[a,b,c] Yong Zhang,[c] Lei Gao,[a] Liping Zeng,[c] Lin Liu,[a] Yanhua Qi,[f] Beixin Mo,[a] and Xuemei Chen[c,1]

[a] Guangdong Provincial Key Laboratory for Plant Epigenetics, Longhua Institute of Innovative Biotechnology, College of Life Sciences and Oceanography, Shenzhen University, Shenzhen 518060, China
[b] Key Laboratory of Optoelectronic Devices and Systems of Ministry of Education and Guangdong Province, College of Optoelectronic Engineering, Shenzhen University, Shenzhen 518060, China
[c] Department of Botany and Plant Sciences, Institute of Integrative Genome Biology, University of California, Riverside, California 92521
[d] State Key Laboratory of Crop Stress Biology for Arid Areas, College of Agronomy, Northwest A&F University, Yangling, Shanxi 712100, China
[e] State Key Laboratory of Plant Physiology and Biochemistry, College of Biological Sciences, China Agricultural University, Beijing 100193, China
[f] State Key Laboratory of Plant Physiology and Biochemistry, College of Life Sciences, Zhejiang University, Hangzhou 310058, China

ORCID IDs: 0000-0003-3960-1746 (S.W.); 0000-0003-3930-4987 (L.Q.); 0000-0002-1903-023X (S.L.); 0000-0002-9935-1892 (C.Y.); 0000-0003-3881-4344 (Y.Z.); 0000-0002-6488-0292 (L.G.); 0000-0002-3579-9145 (L.Z.); 0000-0003-0023-7975 (L.L.); 0000-0002-6234-5317 (Y.Q.); 0000-0001-7279-9788 (B.M.); 0000-0002-5209-1157 (X.C.)

PROTEIN PHOSPHATASE4 (PP4) is a highly conserved Ser/Thr protein phosphatase found in yeast, plants, and animals. The composition and functions of PP4 in plants are poorly understood. Here, we uncovered the complexity of PP4 composition and function in Arabidopsis (*Arabidopsis thaliana*) and identified the composition of one form of PP4 containing the regulatory subunit PP4R3A. We show that *PP4R3A*, together with one of two redundant catalytic subunit genes, *PROTEIN PHOSPHATASE X* (*PPX*)*1* and *PPX2*, promotes the biogenesis of microRNAs (miRNAs). PP4R3A is a chromatin-associated protein that interacts with RNA polymerase II and recruits it to the promoters of miRNA-encoding (*MIR*) genes to promote their transcription. PP4R3A likely also promotes the cotranscriptional processing of miRNA precursors, because it recruits the microprocessor component HYPONASTIC LEAVES1 to *MIR* genes and to nuclear dicing bodies. Finally, we show that hundreds of introns exhibit splicing defects in *pp4r3a* mutants. Together, this study reveals roles for Arabidopsis PP4 in transcription and nuclear RNA metabolism.

INTRODUCTION

PROTEIN PHOSPHATASE4 (PP4) is a highly conserved PP2A-type of Ser/Thr protein phosphatase found in eukaryotes that participates in a variety of cellular events (Cohen et al., 2005; Moorhead et al., 2009). The role of PP4 in DNA damage repair is particularly well documented, and its substrates involved in responses to DNA breaks and replication stress have been identified in animals (Chowdhury et al., 2008; Lee et al., 2010, 2012; Liu et al., 2012). These substrates include the chromatin condensation factor KAP1 (Kruppel-associated box-associated protein 1; Lee et al., 2012; Liu et al., 2012), Replication Protein A2, and the histone H2A variant γ-H2AX (Chowdhury et al., 2008; Lee et al., 2010). Arabidopsis (*Arabidopsis thaliana*) plants carrying mutations in the conserved PP4 regulatory subunit 3 (*PP4R3*) gene, *PLATINUM SENSITIVITY* (*PSY*) *2L/SUPPRESSOR OF MEK1* (*SMEK*)*1*, show enhanced sensitivity to the genotoxic drug cisplatin and exhibit activation of DNA repair signaling genes (Kataya et al., 2017). Thus, PP4 likely functions as a universal regulator of genome integrity.

Arabidopsis mutants in *PSY2L/SMEK1* display pleiotropic phenotypes, strongly suggesting that PP4 plays a role in plant growth and development in addition to its role in DNA damage repair. *PSY2L/SMEK1* was recently found to promote microRNA (miRNA) biogenesis in Arabidopsis (Su et al., 2017). Plant miRNAs are 20–24-nucleotide small RNAs that associate with ARGONAUTE (AGO) proteins (mainly AGO1) to mediate the post-transcriptional silencing of target genes by mRNA cleavage or translational repression. MiRNA biogenesis involves a series of coordinated steps (Rogers and Chen, 2013). DNA-dependent RNA polymerase II (Pol II) transcribes miRNA-encoding genes (*MIR* genes) into primary miRNAs (pri-miRNAs); this step is facilitated by Mediator, Elongator, and transcription factors such as NEGATIVE ON TATA LESS2 (NOT2) and CELL DIVISION CYCLE5 (CDC5; Xie et al., 2005; Zheng et al., 2009; Kim et al., 2011; Wang

[1] Address correspondence to xuemei.chen@ucr.edu and bmo@szu.edu.cn.
The authors responsible for distribution of materials integral to the findings presented in this article in accordance with the policy described in the Instructions for Authors (www.plantcell.org) are: Xuemei Chen (xuemei.chen@ucr.edu) and Beixin Mo (bmo@szu.edu.cn).
www.plantcell.org/cgi/doi/10.1105/tpc.18.00556

et al., 2013; Zhang et al., 2013; Fang et al., 2015). DICER-LIKE 1 (DCL1) processes pri-miRNAs into stem-loop precursors (pre-miRNAs) and then into miRNA/miRNA*duplexes in the nucleus (Kurihara and Watanabe, 2004). DCL1 associates with HYPONASTIC LEAVES 1 (HYL1) and SERRATE (SE) to form the microprocessor or Dicing complex, which is localized to subnuclear foci known as dicing bodies (D-bodies; Fang and Spector, 2007). HYL1 is regulated by phosphorylation/dephosphorylation: phosphorylation might be performed by MITOGEN-ACTIVATED PROTEIN KINASE3 and SUCROSE NONFERMENTING 1-RELATED PROTEIN KINASE2, whereas dephosphorylation by C-TERMINAL DOMAIN PHOSPHATASE-LIKE1, 2 (CPL1/2) is required for accurate miRNA processing (Manavella et al., 2012; Raghuram et al., 2015; Yan et al., 2017). PSY2L/SMEK1 is thought to promote miRNA biogenesis by dephosphorylating HYL1 to enhance its stability (Su et al., 2017).

Little is known about PP4 in Arabidopsis. Studies of the biological and molecular functions of PP4 have been restricted to mutants in *PSY2L/SMEK1* (Kataya et al., 2017; Su et al., 2017). The two genes encoding the putative catalytic subunits, *PROTEIN PHOSPHATASE X1* (*PPX1*) and *PPX2*, have not been characterized genetically. Thus, it is unclear whether the phenotypes of the *psy2l/smek1* mutants reflect the functions of PP4. Biochemical characterization of the composition of PP4 has been limited to the demonstration that PSY2L/SMEK1 interacts with PPX1 and PPX2 in vivo (Su et al., 2017). Here, we report the potential existence of several forms of PP4 and the composition of one PP4 form. *PSY2L/SMEK1* has an un-annotated and expressed homolog in the genome, and thus we named *PSY2L/SMEK1* and this homolog *PP4R3A* and *PP4R3B*, respectively. Immunoprecipitation followed by mass spectrometry analysis with PP4R3A identified PPX1, PPX2, and PP4R2 LIKE (PP4R2L). Each *ppx* single mutant has no obvious phenotypes, but the double mutant resembles *pp4r3a* mutants, suggesting the presence of at least two PP4 forms with either PPX1 or PPX2 as the catalytic subunit. We show that not only *PP4R3A*, but also the catalytic subunit genes *PPX1* and *PPX2*, are required for miRNA biogenesis. We show that PP4R3A is a chromatin-associated protein found at *MIR* genes and that it associates with and recruits Pol II to *MIR* genes to promote their transcription. Furthermore, we demonstrate that PP4 promotes the recruitment of HYL1 to *MIR* genes and the formation of D-bodies. Thus, PP4 coordinates the transcription and processing steps of miRNA biogenesis. Moreover, numerous protein-coding genes show intron retention in two *pp4r3a* mutants, indicating that PP4 plays broader roles in nuclear RNA metabolism.

RESULTS

Isolation of an Arabidopsis Mutant Defective in miRNA Biogenesis

We took advantage of the visible vein-bleaching phenotype of the *SUC2: amiR-SULFUR* (*amiR-SUL*) transgenic line as a readout of miRNA activity to screen for mutants with potential defects in miRNA biogenesis or activity. In the *amiR-SUL* line, a phloem-specific promoter (*SUC2*) drives the expression of an artificial miRNA (amiR-SUL) that targets the *SULFUR* (*SUL*) gene, which is required for chlorophyll biosynthesis, leading to vein-centered leaf bleaching (de Felippes et al., 2011). We isolated a suppressor of *amiR-SUL, sup-e33*, with reduced leaf bleaching (Figure 1A; Supplemental Figure 1A and 1B). This phenotype suggested that *sup-e33* is defective in amiR-SUL biogenesis or activity. Indeed, the levels of amiR-SUL were reduced in the mutant (Figure 1B); concomitantly, the expression of *SUL* was de-repressed, as reflected by both its transcript (Figure 1C) and protein levels (Figure 1D). The *sup-e33* mutant exhibits pleiotropic phenotypes, including smaller plant size, early flowering, defective phyllotaxy and smaller silique-stem angles, and reduced fertility (Supplemental Figure 1). Because impaired miRNA biogenesis causes pleiotropic developmental defects (Park et al., 2002; Grigg et al., 2005; Zhang et al., 2013), we speculated that *sup-e33* might be impaired in miRNA accumulation in general. We thus examined the abundance of endogenous miRNAs in 12-d-old *amiR-SUL* and *sup-e33* seedlings. The accumulation of all miRNAs examined (miR166, miR164, miR159, miR390, miR319, miR172, miR156, and miR168) was reduced in *sup-e33* compared with *amiR-SUL* (Figure 1B). We then examined the expression of seven known miRNA target genes (*SQUAMOSA PROMOTER BINDING PROTEIN-LIKE5*, *PHABULOSA*, *PHAVOLUTA*, *REVOLUTA* [*REV*], *MYELOBLASTOSIS DOMAIN PROTEIN33* [*MYB33*], *AGO1*, and *AUXIN RESPONSE FACTOR8*) by reverse transcription quantitative PCR (RT-qPCR). As expected, the transcript levels of these genes were elevated in *sup-e33* (Figure 1C). In addition, the protein levels of two miRNA targets (SE and AGO2) were elevated in *sup-e33* (Figure 1D). The miRNAs that target these two genes, miR863-3p and miR403, were found to be at lower levels in the mutant based on small RNA-seq (Supplemental Data Set 1). Several miRNAs trigger the production of phased small interfering RNAs (siRNAs) from target genes (Fei et al., 2013; Komiya, 2017). We also detected the accumulation of miR173-triggered phased siRNAs known as trans-acting siRNAs (tasiRNAs; Allen et al., 2005). The levels of TRANS-ACTING SIRNA (TAS1)-siR255 and TAS2-siR1511 were lower in *sup-e33* than in *amiR-SUL* (Figure 1B).

A Mutation in *PP4R3A*, Encoding Regulatory Subunit 3 of PP4, Accounts for Compromised miRNA Accumulation

To identify the mutation in *sup-e33*, we backcrossed *sup-e33* with the parental *amiR-SUL* line. More than 100 F2 segregants with the *sup-33* phenotype were pooled for whole-genome resequencing. A C^{792} -to-T mutation in the open reading frame of AT3G06670 (this mutation is predicted to introduce a premature termination codon) was identified in *sup-e33*. In the F2 population of the backcross, this mutation was present in all 106 mutant plants tested, suggesting genetic linkage between the mutation and the phenotypes of *sup-e33*. We amplified genomic DNA encompassing the promoter and the coding region of AT3G06670 from wild-type plants and fused it to yellow fluorescent protein (YFP). This transgene, when introduced into *sup-e33* plants, completely rescued the mutant phenotypes in terms of both leaf bleaching and miRNA defects (Figures 1A to 1C), confirming that the mutation in AT3G06670 leads to compromised miRNA accumulation. AT3G06670 encodes regulatory subunit 3 of PP4

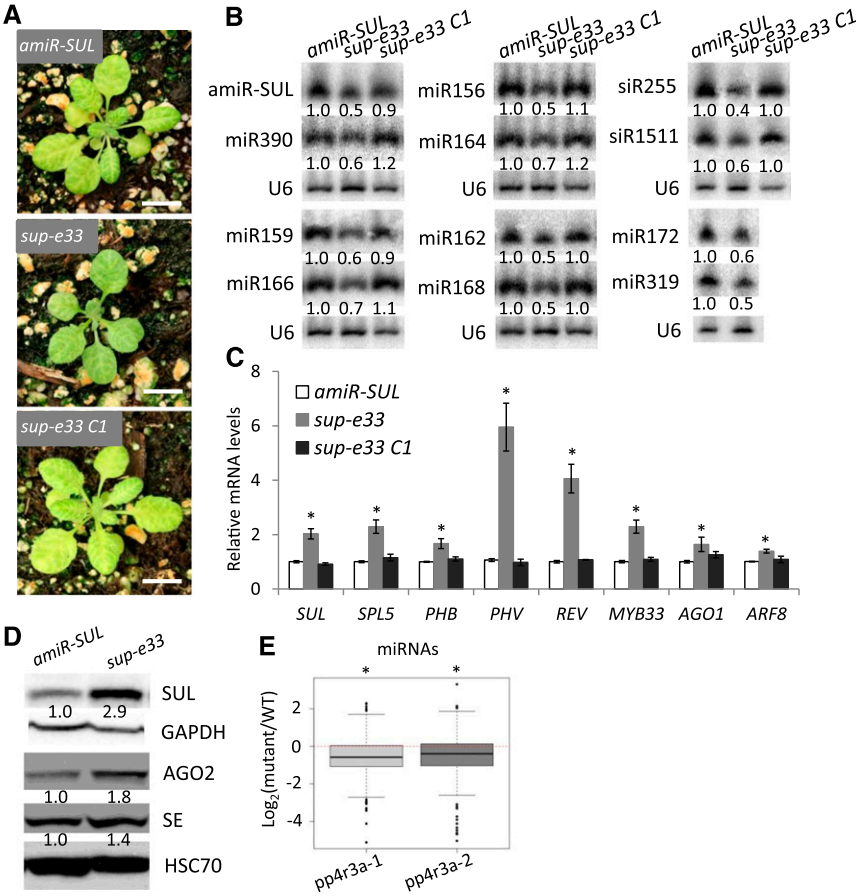

Figure 1. The *sup-e33* Mutant Is Defective in miRNA Biogenesis.

(A) Morphological phenotypes of 3-week-old *SUC2:amiR-SUL* (*amiR-SUL*), *sup-e33*, and rescued *sup-e33* (*sup-e33 C1*) plants. Scale bars = 1 cm.
(B) RNA gel blot analysis to detect various miRNAs and tasiRNAs (siR155 and siR1511) in *amiR-SUL*, *sup-e33*, and rescued *sup-e33* plants. U6 served as a loading control. The numbers represent relative abundance of small RNAs in the three genotypes.
(C) Transcript levels of miRNA targets, as determined by RT-qPCR. *UBIQUITIN5* (*UBQ5*) served as an internal control. Error bars indicate SD from three independent experiments; asterisks indicate significant difference (*t* test, $P < 0.05$).
(D) Protein levels of miRNA targets (SUL/amiR-SUL, SE/miR863-3p, AGO2/miR403) in *sup-e33*, as determined by protein gel blot analysis. Glyceraldehyde 3-phosphate dehydrogenase (GAPDH) and heat shock cognate (HSC)70 served as loading controls.
(E) Global abundance of miRNAs in Col and *pp4r3a* alleles, as determined by small RNA-seq. The small RNAs were normalized against total reads, abundance is expressed as RPM (reads per million mapped reads), and $\log_2$ fold changes (mutant/wild type) were plotted. Asterisk indicates that the mean $\log_2$ fold change is significantly below 0 (Wilcox. test, $P < 2.3e\text{-}10$).

(PP4R3, also known as PSY2L/SMEK1). We will refer to this gene as *PP4R3A* due to the presence of a homolog (see below).

To examine the phenotypes caused by the loss or reduced function of *PP4R3A* in an otherwise wild-type background, we crossed *sup-e33* with wild type (Col) plants and obtained the *pp4r3a-1* allele without the *amiR-SUL* transgene. We also acquired a T-DNA insertion allele, *pp4r3a-2* (also known as *smek1-2*; Su et al., 2017). The *pp4r3a-2* mutant displayed smaller plant size and darker green leaves than *pp4r3a-1* (Figure 2C), suggesting that *pp4r3a-2* has a stronger mutant phenotype than *pp4r3a-1*. In RNA-seq analysis, *PP4R3A* was found to be expressed at much lower levels in *pp4r3a-2* than *pp4r3a-1* and the wild type, suggesting that *pp4r3a-2* is a strong knock-down allele (Supplemental Figure 2). The two mutants also had short roots (Supplemental Figure 3). We performed small RNA-sequencing (sRNA-seq) on 12-day-old Col, *pp4r3a-1* and *pp4r3a-2* seedlings (Figure 2A). Three sets of samples from each genotype were separately processed for library construction and sequencing, and the three independent experiments of the samples from each genotype were found to be reproducible (Supplemental Figure 4). A global reduction in miRNA accumulation was observed in the two *pp4r3a* mutants (Figure 1E; Supplemental Data Set 1), confirming that *PP4R3A* is required for miRNA biogenesis.

In the Arabidopsis genome, three clustered, annotated genes, AT5G49370, AT5G49380, and AT5G49390, share similarity to the *N*-terminal, middle, and *C*-terminal portions of *PP4R3A*, respectively. This observation suggested that the three "genes" could actually be one gene, which would be a homolog of *PP4R3A*.

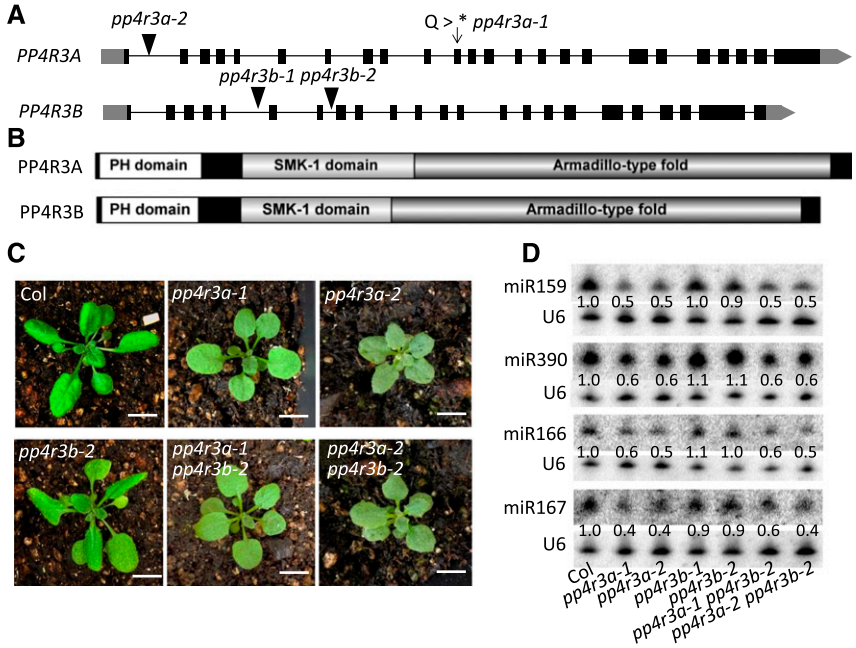

Figure 2. Gene Cloning and Genetic Characterization of *PP4R3A* and *PP4R3B*.

(A) Gene structures of *PP4R3A* and *PP4R3B* (gray block, untranslated region; black blocks, exons; black lines, introns). The arrow indicates the point mutation site in *sup-e33* (designated as *pp4r3a-1*), and the black triangles indicate the T-DNA insertion sites.
(B) Both PP4R3A and PP4R3B possess a pleckstrin homology (PH) domain, a suppressor of MEK-1 (SMK-1) domain, and an Armadillo fold.
(C) Morphological phenotypes of 3-week-old Col, *pp4r3a-1* (*sup-e33* in Col background), *pp4r3a-2*, *pp4r3b-2*, *pp4r3a-1 pp4r3b-2*, and *pp44r3a-2 pp4r3b-2* plants. Scale bars = 1 cm.
(D) Determination of miRNA levels in *pp4r3a*, *pp4r3b* and *pp4r3a pp4r3b* by RNA gel blot analysis of small RNAs. The numbers represent relative abundance of small RNAs.

Indeed, a full-length transcript containing all three "genes" was obtained by RT-PCR and sequenced. The protein encoded by this transcript is highly similar in domain composition to the protein encoded by *PP4R3A* (Figures 2A and 2B). Thus, the three annotated genes actually represent one gene, which we named *PP4R3B*. We generated transgenic plants harboring the β-glucuronidase (GUS) reporter driven by the *PP4R3A* promoter and found that *PP4R3A* was mainly expressed in vascular tissue, with higher expression in roots than shoots (Supplemental Figure 5A). The promoter activity of *PP4R3B* was detectable in vascular tissue and mesophyll cells, but not in actively growing tissues such as young leaves or lateral root primordia (Supplemental Figure 5B).

To investigate whether *PP4R3A* and *PP4R3B* play redundant roles in morphogenesis and miRNA biogenesis in Arabidopsis, we obtained T-DNA insertion lines in *PP4R3B*; these alleles were named *pp4r3b-1* and *pp4r3b-2*, respectively (Figure 2A). Neither *pp4r3b* allele had any obvious mutant phenotypes. The *pp4r3a-1 pp4r3b-2* and *pp4r3a-2 pp4r3b-2* double mutants resembled the corresponding *pp4r3a* single mutants in terms of plant morphology and in miRNA accumulation (Figures 2C and 2D), suggesting that *PP4R3B* does not play an overlapping role with *PP4R3A* in Arabidopsis development or miRNA biogenesis. We also introduced *PP4R3B-YFP* driven by the constitutive CaMV 35S promoter into *pp4r3a-1* plants. The 11 transgenic T1 plants showed different levels of *PP4R3B-YFP* expression, but none of them exhibited morphological phenotypes indicative of transgene rescue of *pp4r3a-1* (Supplemental Figure 6). These results suggest that *PP4R3B* cannot substitute for *PP4R3A* in terms of plant development or miRNA biogenesis. Because *PP4R3B* is expressed, it likely has an as-yet unknown function.

The PP4 Catalytic Subunits Promote miRNA Biogenesis

In the yeast *Saccharomyces cerevisiae* and mammals, PP4R3/Psy2 was identified as regulatory subunit 3 of the PP4 complex, which also contains the catalytic subunit (PP4C) and regulatory subunit 2 (PP4R2; Gingras et al., 2005; Hastie et al., 2006). To uncover the composition of the Arabidopsis PP4 complex, we introduced the *PP4R3A:PP4R3A-YFP* and *PP4R3A:PP4R3A-HEMAGGLUTININ* (*HA*) transgenes, respectively, into the *pp4r3a-1* background. The transgenes were functional, because they fully rescued the morphological defects of the mutant (Supplemental Figure 7). We then immunoprecipitated (IP) PP4R3A-YFP from *PP4R3A:PP4R3A-YFP/pp4r3a-1* plants and PP4R3A-HA from *PP4R3A:PP4R3A-HA/pp4r3a-1* plants. In both experiments, Col plants were included as the negative control. Mass spectrometry (MS) analysis of the immunoprecipitates showed that PP4R3A associates with two catalytic subunits, PPX1 and PPX2, and the regulatory subunit PP4R2L (Supplemental Figure 8A and Supplemental Data Set 2). To determine whether PP4 acts in

miRNA biogenesis, we searched for mutants in the catalytic subunit. However, T-DNA insertion mutants in *PPX1* or *PPX2* genes were not available. We therefore performed CRISPR/Cas9 (clustered regularly interspaced short palindromic repeats/CRISPR-associated endonuclease9)-based gene editing (Yan et al., 2015) and successfully obtained *ppx1* and *ppx2* single mutants with base deletions (Supplemental Figure 8B). Neither single mutant showed any morphological defects (Figure 3A). In the F2 population of the cross between the two mutants, we found only three tiny seedlings displaying similar phenotypes to those of *pp4r3a-2* among ~150 seedlings (Figure 3A); these tiny plants indeed were *ppx1 ppx2* double mutants, as revealed by genotyping. However, the proportion of double mutants in the F2 population was so low that we speculated that most of the double mutants were embryo lethal. Consistent with this hypothesis, we observed defective embryos in the siliques of *ppx1*/*ppx1 PPX2*/*ppx2* plants (Supplemental Figure 8C). This finding suggests that the two *PPX* genes play largely redundant roles and together are essential, implying that either PPX protein assembles a PP4 complex. We harvested viable *ppx1 ppx2* seedlings from the progeny of *ppx1*/*ppx1 PPX2*/*ppx2* plants and measured the levels of mature miRNAs. Although both *ppx* single mutants resembled the wild type, the double mutant showed reduced levels of mature miRNAs and TAS1-siR255 (Figure 3B). Therefore, the biochemical and genetic data demonstrate that at least two subunits of the PP4 complex (PP4R3A and PPX) participate in miRNA biogenesis.

PP4R3A Has Effects beyond Pri-miRNA Processing in miRNA Biogenesis

PP4R3A was previously reported to stabilize the DCL1 co-factor HYL1 and promote pri-miRNA processing; in two mutants in this gene, HYL1 protein levels were reduced to approximately half of wild-type levels (Su et al., 2017). However, we did not observe a reduction in HYL1 protein levels in *pp4r3a-1* or *pp4r3a-2* (this allele is the same as *smek1-2*; Su et al., 2017). In fact, an increase in HYL1 protein levels was observed at the normal growth temperature in the two alleles, although HYL1 protein levels were slightly reduced in *pp4r3a-1* at 30°C (Supplemental Figure 9B). The lack of reduction in HYL1 protein levels in the *pp4r3a* mutants at 22°C suggested that the reduced miRNA abundance in the mutants is not solely attributable to defects in pri-miRNA processing. To examine this notion genetically, we crossed *sup-e33* (*pp4r3a-1 amiR-SUL*) plants with mutants in the core dicing complex genes *DCL1*, *HYL1*, and *SE* in the *amiR-SUL* background. As expected, the *dcl1-20*, *hyl1-2*, and *se-1* mutations compromised leaf bleaching in the *amiR-SUL* background (Figures 4A to 4D), which is consistent with the reduced levels of amiR-SUL in these backgrounds (Figure 4E). The double mutants had even lower levels of amiR-SUL compared with each single mutant (Figure 4E). The morphological phenotypes of the double mutants were also more severe than those of the corresponding single mutants (Figures 4A to 4D). The accumulation of endogenous miRNAs in the double mutants tended to further decrease compared with the corresponding single mutants (Supplemental Figure 10). Although the *dcl1-20* and *se-1* alleles are not null alleles (null alleles in these genes are embryo lethal; Golden et al., 2002; Grigg et al., 2005; Armenta-Medina et al., 2017), the *hyl1-2* allele is likely a null allele, because no HYL1 protein was detected in this mutant (Cho et al., 2014). The finding that *pp4r3a-1* enhanced the miRNA biogenesis defects of *hyl1-2* indicates that *PP4R3A* plays a role in miRNA biogenesis beyond its reported role in stabilizing HYL1 protein.

PP4R3A Promotes the Transcription of *MIR* Genes

To determine the potential reasons for reduced miRNA accumulation in the *pp4r3a* mutants, we examined the expression of

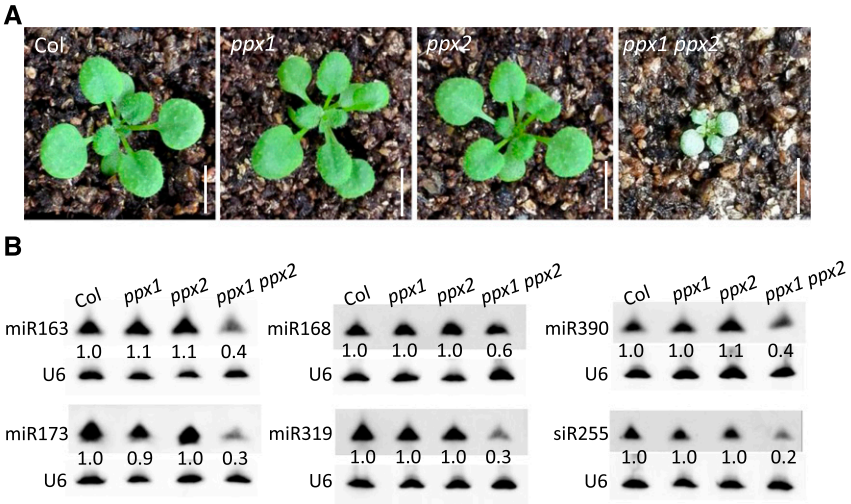

Figure 3. Phenotypes of PP4 Catalytic Mutants.

(A) Morphologic phenotypes of the *ppx1* and *ppx2* single mutants and the *ppx1 ppx2* double mutant. Scale bars = 1 cm.
(B) Accumulation of miRNAs and an siRNA in Col, *ppx1*, *ppx2*, and *ppx1 ppx2* plants as detected by RNA gel blot analysis of small RNAs. U6 served as a loading control. The numbers indicate relative abundance of the small RNAs in the four genotypes.

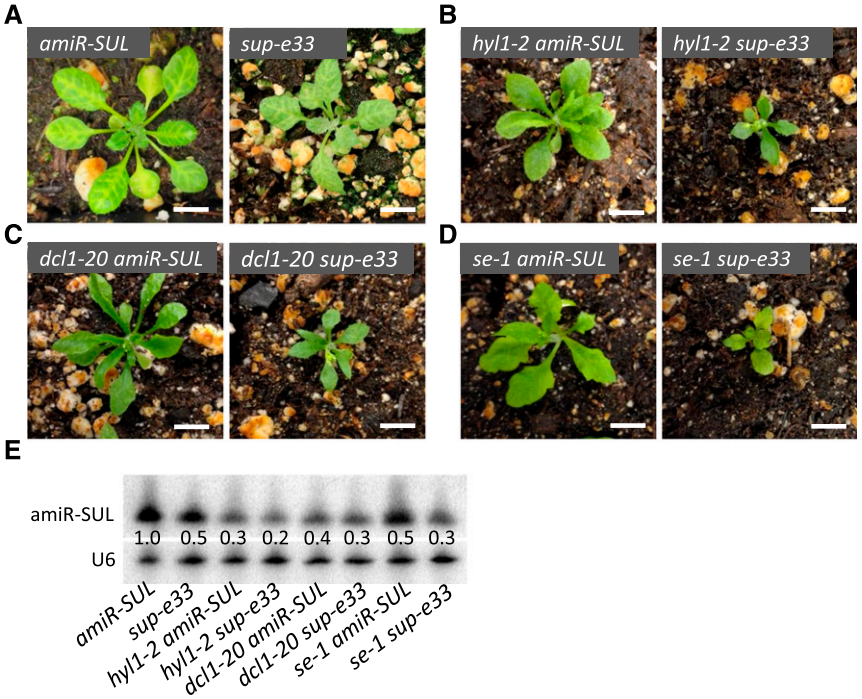

Figure 4. Genetic Interactions between *sup-e33* and Pri-miRNA Processing Mutants.

(A) to (D) Morphological phenotypes of 3-week-old plants of the indicated genotypes. Scale bars = 1 cm.
(E) RNA gel blot analysis of small RNAs to determine the levels of amiR-SUL in various genotypes. U6 served as a loading control. The numbers represent relative abundance.

known components in the miRNA biogenesis machinery. No changes in the transcript levels of these genes were found in the *pp4r3a* mutants (Supplemental Figure 9A). Moreover, the protein levels of some important factors in miRNA biogenesis, such as Pol II, HYL1, and SE, were not substantially reduced or were even increased (such as HYL1 and SE at 22°C) in the *pp4r3a* mutants compared with wild type (Supplemental Figure 9B). AGO1 protein levels were reduced in the two *pp4r3a* mutants (Supplemental Figure 9B), which is consistent with the global reduction in miRNA accumulation. We then examined the levels of HYL1, SE, and AGO1 at different growth temperatures. Intriguingly, the increase in HYL1 levels in *pp4r3a-1* detected at 22°C and 16°C was not observed at 30°C, whereas the increase in SE levels detected at 22°C and 30°C was not observed at 16°C (Supplemental Figure 9B). These observations suggest that PP4R3A plays a role in the responses of plants to different temperatures, which deserves further investigation in the future.

We then examined the transcript levels of 13 pri-miRNAs and found that the abundance of the tested pri-miRNAs, except for pri-miR164a and pri-miR157a, was drastically reduced in both *pp4r3a* alleles and *ppx1 ppx2*. The transcript levels of pri-miR164a and pri-miR157a were also reduced in *pp4r3a-2* and *ppx1 ppx2*, although their levels were not obviously changed in *pp4r3a-1* (Figure 5A). These results suggest that PP4 promotes the transcription of *MIR* genes. We examined the activities of *MIR* gene promoters in *pp4r3a-1*. We crossed two transgenic lines harboring the *GUS* reporter gene driven by the *MIR167a* or *MIR172b* promoter in the wild-type background with *pp4r3a-1* plants and compared the expression of homozygous and isogenic transgenes between wild-type and *pp4r3a-1* plants. GUS activity was greatly reduced in *pp4r3a-1*, as revealed by GUS staining. RT-qPCR analysis confirmed that *GUS* mRNA levels were reduced in *pp4r3a-1* (Figures 5B and 5C), indicating that the transcription of *MIR* genes is impaired in *pp4r3a-1*. Consistent with the role of *PP4R3A* in *MIR* gene transcription, crosses with two other mutants with reduced transcription of *MIR* genes, *nuclear rna polymerase II* (*nrpb*)*2-3* (Zheng et al., 2009) and *cdc5-1* (Zhang et al., 2013), enhanced the weaker *pp4r3a-1* mutant in terms of both plant morphology and miRNA levels (Figures 5D and 5E). In fact, the *nrpb2-3 pp4r3a-1* and *cdc5-1 pp4r3a-1* double mutants resembled the *pp4r3a-2* allele, a strong knockdown allele (Figures 5D and 5E).

PP4R3A Associates with Chromatin and Is Required for Pol II Occupancy at *MIR* Promoters

A classical bipartite-type nuclear localization signal is present in the Armadillo domain of PP4R3A. In *PP4R3A:PP4R3A-YFP/pp4r3a-1* transgenic plants, YFP fluorescence was present in only the nucleus (Figure 6A). Given the finding that PP4R3A promotes *MIR* transcription and its known role in DNA damage repair, we wondered whether this protein is associated with chromatin. Using *PP4R3A:PP4R3A-HA/pp4r3a-1* transgenic plants, we performed cytoplasmic/nuclear fractionation and extracted chromatin from the nuclear fraction. Protein gel blot analysis

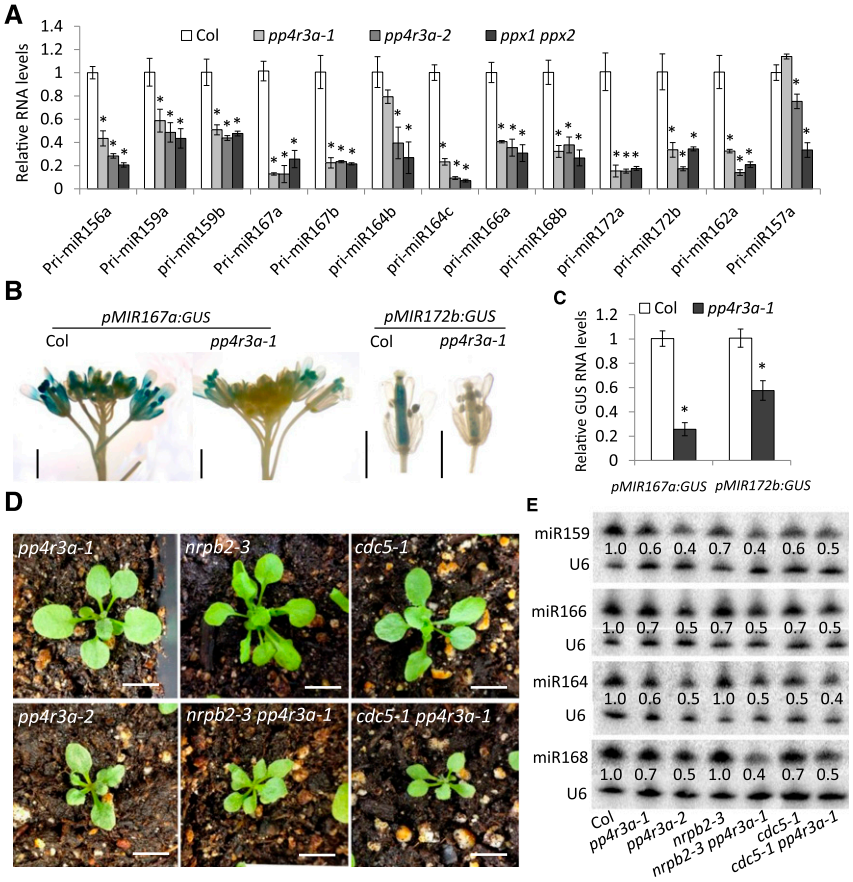

Figure 5. Requirement of PP4R3A for *MIR* Transcription.

(A) Determination of pri-miRNA levels by RT-qPCR.
(B) GUS staining of representative samples harboring *pMIR167a:GUS* and *pMIR172b:GUS* in the Col and *pp4r3a-1* backgrounds. Scale bars = 2 mm.
(C) *GUS* transcript levels in samples harboring *pMIR167a:GUS* and *pMIR172b:GUS* in the Col and *pp4r3a-1* backgrounds, as determined by RT-qPCR.
(D) and **(E)** Genetic interactions between mutations in *PP4R3A*, *NRPB2* and *CDC5*. **(D)** Additive phenotypes of *nrpb2-3 pp4r3a-1* and *cdc5-2 pp4r3a-1* double mutants. Scale bars = 1 cm. Note that the phenotypes of the double mutants were much stronger than the corresponding single mutants, but similar to that of *pp4r3a-2*. **(E)** The abundance of miRNAs in Col, *pp4r3a-1*, *pp4r3a-2*, *nrpb2-3*, *cdc5-1*, *nrpb2-3 pp4r3a-1*, and *cdc5-1 pp4r3a-1*, as detected by RNA gel blot analysis of small RNAs.
In **(A)** and **(C),** *UBQ5* served as the internal control; error bars indicate SD from three independent experiments; asterisks indicate significant difference (*t* test, $P < 0.05$).

showed the presence of PP4R3A-HA in the nuclear rather than the cytoplasmic fraction, and also revealed its association with chromatin (Figure 6B). Because PP4R3A is required for *MIR* promoter activity, we examined whether PP4R3A binds *MIR* promoters. We performed chromatin immunoprecipitation (ChIP) assay with Col and *pPP4R3A:PP4R3A-HA/pp4r3a-1* plants using an anti-HA antibody. Promoter regions of the tested *MIRs* were enriched in the immunoprecipitates from *pPP4R3A:PP4R3A-HA/pp4r3a-1* plants (Figure 6C), indicating that PP4R3A is associated with *MIR* promoters.

MIR genes are transcribed by Pol II (Xie et al., 2005; Zheng et al., 2009). To determine whether PP4R3A associates with Pol II, we tagged the largest subunit of Pol II (RPB1) with the MYC epitope, crossed *RPB1-MYC* plants with *PP4R3A-YFP/pp4r3a-1* plants, and extracted proteins from F1 plants expressing both RPB1-MYC and PP4R3A-YFP for co-immunoprecipitation (Co-IP). Reciprocal Co-IP was conducted and protein gel blot analysis showed that RPB1-MYC and PP4R3A-YFP was effectively enriched using anti-MYC antibody and green fluorescent protein (GFP)-Trap, respectively, and that RPB1-MYC was present in PP4R3A-YFP immunoprecipitates and vice versa (Figure 6D). Then, we analyzed the occupancy of Pol II at *MIR* promoters by ChIP, which was conducted on *RPB1-MYC* transgenic plants in Col (*RPB1-MYC*) and *pp4r3a-1* (*RPB1-MYC pp4r3a-1*) backgrounds using an anti-MYC antibody. The promoter regions of all tested *MIRs* were enriched in *RPB1-MYC* and *RPB1-MYC pp4r3a-1* immunoprecipitates; however, the enrichment fold in *RPB1-MYC pp4r3a-1* was significantly reduced when compared with that in *RPB1-MYC* (Figure 6E). Taken together, these data show that PP4R3A promotes the transcription of *MIR* genes through recruitment of Pol II to *MIR* promoters.

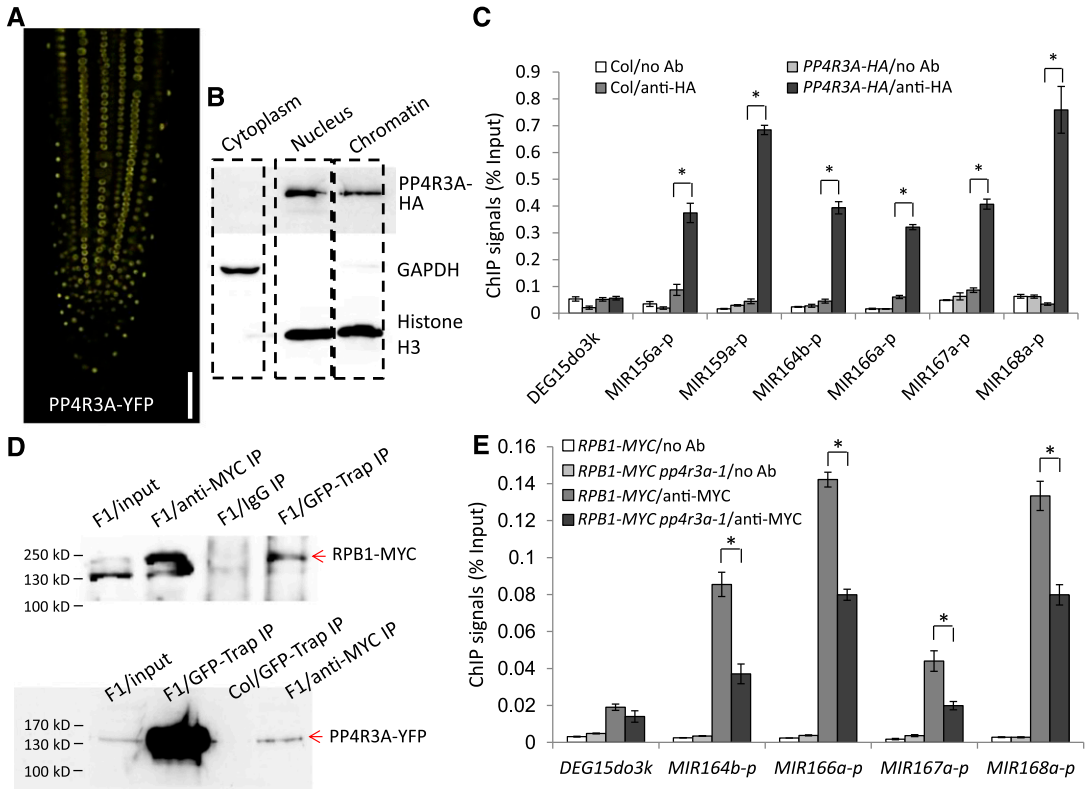

Figure 6. Analysis of *PP4R3A* Localization and Pol II Occupancy at *MIR* Promoters.

(A) YFP signals in the root of a 5-d-old *PP4R3A:PP4R3A-YFP* seedling. Scale bar = 200 μm.
(B) Protein gel blot analysis showing the cytoplasmic, nuclear, and chromatin distribution of the PP4R3A-HA protein from a *PP4R3A:PP4R3A-HA*/*pp4r3a-1* transgenic line. GAPDH and histone H3 were used as protein markers for the cytoplasmic and nuclear/chromatin fractions, respectively.
(C) ChIP-qPCR analysis to determine the occupancy of PP4R3A at *MIR* promoters. ChIP was performed with no antibody (no Ab) or anti-HA antibody in Col and *PP4R3A:PP4R3A-HA* transgenic plants.
(D) Co-immunoprecipitation of PP4R3A with Pol II. F1 plants from a cross between *PP4R3A:PP4R3A-YFP* and *RPB1:RPB1-4xMYC* homozygous transgenic lines were used to perform IP, using either anti-MYC or GFP-Trap antibodies. Protein gel blot analysis to detect PP4R3A–YFP and RPB1-MYC was performed with anti-GFP and anti-MYC antibodies, respectively. The protein ladder is labeled on the left.
(E) ChIP-qPCR analysis to determine the occupancy of Pol II at *MIR* promoters using plants with a homozygous *RPB1:RPB1-4xMYC* transgene in the Col and *pp4r3a-1* backgrounds. The intergenic region DEG15do3k between AT1G28310 and AT1G28320 was used as a negative control. The ChIP signal was normalized against input.
In **(C)** and **(E)**, error bars indicate SD from three independent experiments; asterisks indicate significant difference (*t* test, $P < 0.05$).

PP4R3A Promotes HYL1 Localization to D-Bodies and Its Association with *MIR* Loci

In mammals and plants, microprocessor and/or pri-miRNA transcripts are associated with chromatin and the processing of pri-miRNAs occurs co-transcriptionally (Morlando et al., 2008; Ballarino et al., 2009; Fang et al., 2015). In Arabidopsis, both DCL1 and HYL1 can be detected at *MIR* gene loci, suggesting co-transcriptional processing (Fang et al., 2015). We proposed that disruption of *MIR* transcription may affect co-transcriptional pri-miRNA processing. We crossed a *HYL1-YFP* line with *pp4r3a-1* to generate *HYL1-YFP pp4r3a-1* and compared the number of D-bodies in wild type and mutant backgrounds. The number of HYL1-YFP-containing D-bodies was dramatically reduced in *pp4r3a-1* (Figures 7A and 7B), demonstrating that PP4R3A plays a role in the proper localization of HYL1 to D-bodies. To further confirm a defect in pri-miRNA co-transcriptional processing in *pp4r3a-1*, we performed HYL1 ChIP using anti-HYL1 antibodies. HYL1 was detected at the *MIR* loci, and its occupancy at four of five tested *MIR* loci was significantly reduced in *pp4r3a-1* (Figure 7C). These results suggest that PP4R3A is required for the formation of D-bodies and the recruitment of HYL1 to *MIR* genes. Because both PP4R3A and HYL1 are found at *MIR* loci, we entertained the possibility that HYL1, by binding to nascent pri-miRNAs, recruits PP4R3A to *MIR* loci. We performed PP4R3A ChIP-qPCR at eight *MIR* promoters using *PP4R3A:PP4R3A-HA* transgenic plants in the wild type and *hyl1-2* backgrounds and found no significant difference in PP4R3A occupancy at these promoters except for two (Supplemental Figure 11A). Thus, it is likely that PP4R3A recruits HYL1 to *MIR* loci but not vice versa. To determine whether PP4R3A recruits HYL1 to *MIR* loci

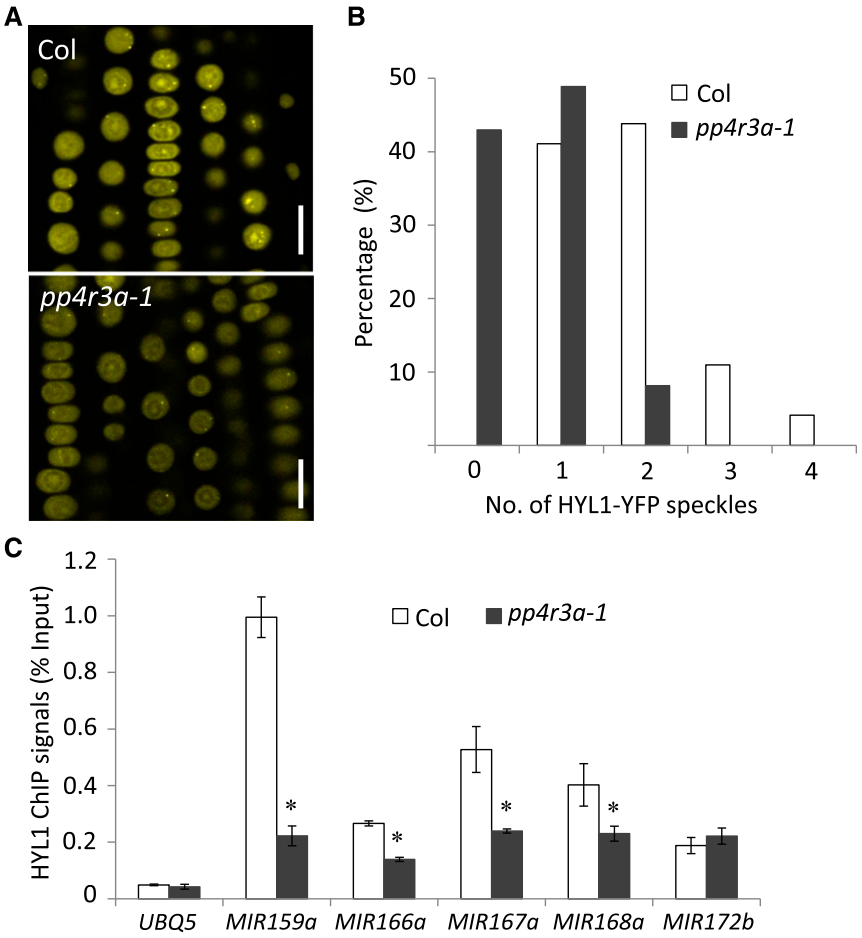

Figure 7. HYL1 Localization and Chromatin Association are Impaired in *pp4r3a-1*.

(A) Representative confocal images of HYL1-YFP fluorescence in the meristematic zones of Col and *pp4r3a-1* roots. Bars = 10 μm.
(B) Quantification of HYL1-YFP D-bodies. The *x* axis represents the number of HYL1-YFP D-bodies (speckles) per cell, and the *y* axis indicates the percentage of cells with the corresponding HYL1-YFP D-body numbers. The number of HYL1-YFP D-bodies was calculated from 146 root cells of Col and 135 root cells of *pp4r3a-1*.
(C) ChIP-qPCR assay to determine the association of HYL1 with *MIR* gene bodies in Col and *pp4r3a-1*. Error bars indicate SD from three independent experiments; asterisk indicates significant difference (*t* test, $P < 0.05$).

through protein-protein interaction, we conducted Co-IP assays. PP4R3A-GFP was immunoprecipitated with GFP-Trap, and the immunoprecipitates were probed for HYL1 and SE by protein gel blot analysis. The two microprocessor components were not detected in the PP4R3A IP (Supplemental Figure 11B).

PP4R3A Promotes Transcription of Protein Coding Genes and Splicing of a Set of Introns

The association between PP4R3A and Pol II raised the possibility that PP4R3A affects the expression of other genes in addition to *MIR* genes. We therefore performed RNA-seq analysis of wild type, *pp4r3a-1*, and *pp4r3-2* plants in three separate experiments. Clustering analysis showed that the replicates of each genotype were reproducible (Supplemental Figure 12A). First, we examined the abundance of pri-miRNAs. Among the 325 annotated pri-miRNAs in Araport11, those that were represented by reads of FPKM>2 were retained. These pri-miRNAs tended to accumulate to lower levels in both mutants compared with wild type (Supplemental Figure 12C). Because some pri-miRNAs overlapped with protein-coding genes, reads from the nearby genes could be mistakenly assigned to the pri-miRNAs. We therefore examined the pri-miRNAs without overlapping protein-coding genes. The levels of these pri-miRNAs were also reduced in both mutants compared with wild type (Supplemental Figure 12C), confirming that PP4R3A is a positive regulator of pri-miRNA accumulation. We then identified differentially expressed genes in each mutant relative to wild type. More than 1000 up- or downregulated genes were found in each *pp4r3a* mutant, and a large overlap was found for the up- or downregulated genes between the two mutant alleles (Figure 8A). Because the presence of allele-specific mis-regulated genes could be due to morphological differences between the two mutants, these genes were not

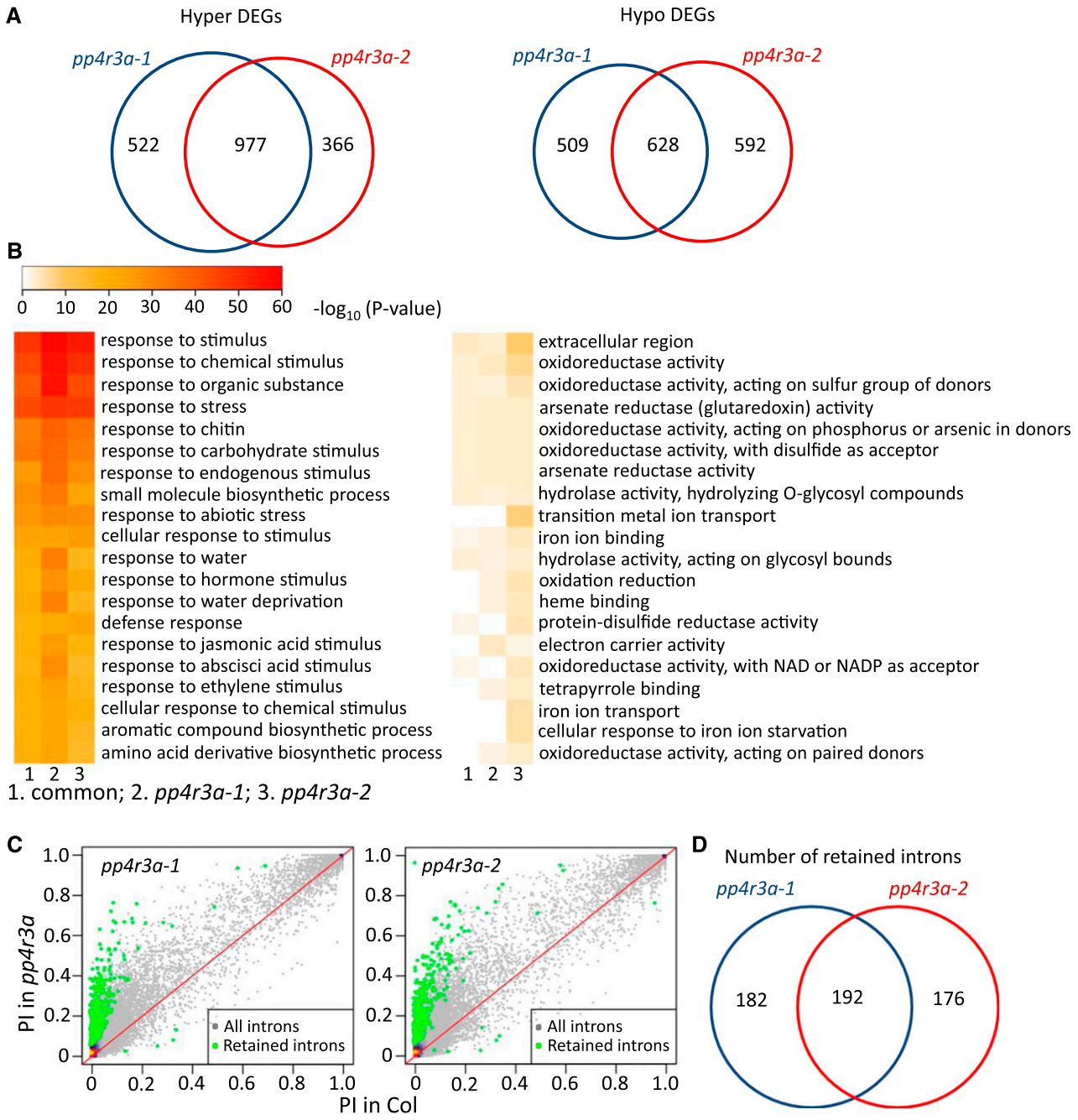

Figure 8. Defects in Gene Expression and Splicing of Pre-mRNAs in *pp4r3a* Mutants.

(A) Venn diagrams showing the number of differentially expressed genes (DEGs) in each *pp4r3a* allele and the overlap of DEGs in the two alleles. Hyper- and hypo-DEGs are genes with increased and decreased expression, respectively.

(B) Gene Ontology enrichment analysis of common DEGs in the two *pp4r3a* alleles. In the *pp4r3a* mutants, upregulated genes are enriched in various stress responses Gene Ontology terms, whereas downregulated genes are involved in oxidation-reduction processes, cellular ion metabolism, and signaling.

(C) Scatterplots showing increased PI (percent of intron reads) in each *pp4r3a* mutant vs. wild type. Each dot represents an annotated intron in Araport11. The introns with a statistically significant increase in PI are shown in green.

(D) Venn diagram showing the number of introns with splicing defects in *pp4r3a-1* and *pp4r3a-2* and the overlap between the two alleles.

investigated further. The overwhelming majority of genes that were upregulated in both alleles were enriched in genes that respond to various stimuli (Figure 8B), suggesting that PP4R3A suppresses plants' responses to various stimuli under normal conditions. This finding appears to be consistent with the observation that *pp4r3a* mutants are more sensitive to abscisic acid treatment than the wild type (Su et al., 2017). The genes that were downregulated in both alleles are involved in cellular oxidation-reduction processes, ion metabolism/transport, and signaling (Figure 8B). Surprisingly, despite the global reduction in miRNA levels in the mutants and the finding that several miRNA target transcripts were upregulated, as revealed by RT-qPCR (Figure 1C), a global trend of upregulation was not observed for known miRNA target genes (Supplemental Figure 12B). One possible explanation is that PP4R3A is also required for the transcription of these genes.

There is emerging evidence linking the processes of miRNA biogenesis and pre-mRNA splicing. On the one hand, introns or 5′ splice sites in some pri-miRNAs stimulate miRNA biogenesis (Bielewicz et al., 2013; Szweykowska-Kulińska et al., 2013). On the other hand, some proteins affect both miRNA biogenesis and the splicing of protein-coding genes, such as the microprocessor component SE, the Cap binding Complex components ABA HYPERSENSITIVE1/CAP-BINDING PROTEIN 80 and CAP-BINDING PROTEIN 20 (Laubinger et al., 2008), the splicing factors STABILIZED1, Arginine/serine (RS)-rich proteins RS40 and RS41 (Ben Chaabane et al., 2013; Chen et al., 2013, 2015), the K-homology domain RNA binding protein HOS5 (Chen et al., 2013, 2015), the proline-rich protein SICKLE (Zhan et al., 2012), and Modifier of snc1, 4-Associated Complex (MAC) components MAC3A, MAC3B, MAC7, PLEIOTROPIC REGULATORY LOCUS1 (PRL1), and PRL2 (Jia et al., 2017; Li et al., 2018). This prompted us to analyze whether the *pp4r3a* mutants show splicing defects. We analyzed splicing defects in the mutants based on RNA-seq data (see Methods for details). Each allele showed an increase in intron retention at more than 350 introns. This number is small considering that more than 70,000 introns were included in the analyses. Retention in both mutants was shown in 192 introns, and a large proportion of the genes with intron retention defects encode proteins that are targeted to organelles (Figures 8C and 8D; Supplemental Figure 13A and 13B). We then analyzed the expression of the genes with intron retention defects. No differential expression of these genes was observed between the wild type and *pp4r3a* mutants (Supplemental Figure 13C). Thus, there was no correlation between intron retention and gene expression levels at these genes. Because the MAC subunits MAC3A, MAC3B, PRL1, and PRL2 also promote intron splicing, we asked whether they affect the same introns as PP4R3A. We analyzed intron retention defects in the *mac3* and *prl* mutants using the same method as for *pp4r3a*. As expected, a significant overlap (hypergeometric test, $P < 9.93E\text{-}62$) was found between the retained introns in *mac3a mac3b* and *prl1 prl2* (Supplemental Figure 13D). There was also significant overlap in retained introns between the *pp4r3a* mutants and the *mac* mutants, but very few commonly affected introns were identified (Supplemental Figure 13D). We examined whether the introns with retention defects in the *pp4r3a* mutants had any common features. When compared with all introns, those with intron retention defects did not differ in terms of their positions along genes. The genes with intron retention defects did not differ from all Arabidopsis genes in terms of the number of introns. However, the introns with retention defects in the mutants tended to be longer as compared with the overall length distribution of introns (Supplemental Figure 14).

DISCUSSION

PP4, a Ser/Thr-specific phosphoprotein phosphatase (PP) conserved from yeast to mammals, is a heteromultimeric complex containing a catalytic subunit (PP4C) and two regulatory/scaffolding subunits, PP4R2 and PP4R3 (Gingras et al., 2005). Genes encoding homologs of all three subunits are present in plants, but our knowledge of the plant PP4 complex is rather limited. Little has been known about the composition of plant PP4 except that PP4R3 interacts in vivo with PPX1 and PPX2, two homologs of PP4C (Su et al., 2017). Reports of PP4 functions in plants were primarily based on studies of PP4R3, also known as PSY2L/SMEK1, in Arabidopsis (Kataya et al., 2017; Su et al., 2017). The current findings shed light on the composition and functions of Arabidopsis PP4. First, through IP of PP4R3 followed by mass spectrometry, we showed that PPX1, PPX2, and the PP4R2 homolog PP4R2L associate with PP4R3A in vivo. Second, through genetic analysis of the *ppx1* and *ppx2* single and double mutants, we showed that the two catalytic subunit genes are largely redundant and that the double mutant resembles the strong *pp4r3a-2* mutant in terms of both morphological and molecular defects. This observation confirms that the PPX proteins function together with PP4R3A in vivo and suggests the presence of two PP4 forms, one containing PPX1 and PP4R3 and the other containing PPX2 and PP4R3. We also found that, in addition to *PP4R3A*, the Arabidopsis genome contains a second gene, which we named *PP4R3B*, which may encode regulatory subunit 3 of another form of PP4. We showed that only *PP4R3A* is critical for plant development and miRNA accumulation under normal growth conditions. *PP4R3B* is expressed and may exert functions under specific conditions.

Evolutionary analysis of PP catalytic subunits has shown that Arabidopsis PP4, like that of other eukaryotes, forms a distinct cluster with PP2A and PP6, which are members of the PP family (Moorhead et al., 2009; Lillo et al., 2014). The regulatory partners of PPs usually modulate the activity and substrate specificity of the catalytic subunits. However, it can be risky to study the functions of regulatory subunits as a substitute for PPs in plants. The Arabidopsis Tap46 (the homolog of yeast and mammalian Tap42/α4), a downstream effector of the target of the rapamycin signaling pathway, is a regulatory subunit that interacts with PP2A and PP2A-related phosphatases PP4 and PP6 with different affinities and plays essential roles in plant growth and responses to chilling (Harris et al., 1999; Ahn et al., 2011). Thus, the functions of Tap46 could reflect those of multiple PPs. In the case of PP4R3A, our IP MS analysis did not detect in vivo interactions with PP2A-type PPs. This observation, together with the similar phenotypes of *pp4r3a-2* and *ppx1 ppx2* mutants, suggests that PP4R3A serves as a specific regulatory subunit of PP4.

Several studies have revealed post-translational modifications of components of the miRNA biogenesis machinery, such as HYL1 and AGO1 (Cho et al., 2016). The double-stranded RNA binding

protein, HYL1, forms a complex with DCL1 and SE to promote precise DCL1 cleavage as well as strand selection during AGO1 loading (Dong et al., 2008; Eamens et al., 2009). Manavella et al. (2012) showed that the dephosphorylation of HYL1 by a family of CPL phosphatases is required for its activity. Unlike the other components of the microprocessor, HYL1 is a short-lived protein that is degraded in the cytoplasm in the dark (Cho et al., 2014). The HYL1 phosphoisoforms (phosphorylated and nonphosphorylated) appear to affect the stability of the protein, as shown in two studies (Su et al., 2017; Achkar et al., 2018). However, these two studies led to different conclusions. One found that phosphorylated HYL1 forms a nuclear reserve of inactive protein protected from dark-induced degradation, whereas dephosphorylated HYL1 is unstable (Achkar et al., 2018). The other study (Su et al., 2017) found that PP4R3A stabilizes HYL1 by dephosphorylating it. Evidence supporting this claim includes the reduced HYL1 levels in the *pp4r3a* mutants and the finding that recombinant HYL1 is more unstable when incubated with *smek1-1* lysates compared with wild-type lysates (Su et al., 2017). Under our growth conditions, we found an increase in HYL1 levels in two *pp4r3a* mutants (including one used in the Su et al. study) compared with wild type, but a small reduction in HYL1 levels was observed in the mutants at higher temperature. These conflicting observations suggest that HYL1 is regulated in an intricate manner in response to environmental conditions.

Emerging evidence suggests that pri-miRNAs are cotranscriptionally processed in plants. NOT2 (a core member of the CARBON CATABOLITE REPRESSION4 [CCR4]-NOT complex; Wang et al., 2013), PRL1, PRL2, CDC5, MAC3A, MAC3B and MAC7 (subunits of the Modifier of snc1, 4-associated complex; Zhang et al., 2013, 2014; Jia et al., 2017; Li et al., 2018), and ELP2 and ELP5 (subunits of the Elongator complex; Fang et al., 2015) interact with Pol II and/or the dicing complex to coordinate *MIR* transcription and pri-miRNA processing. We found that mutations in *PP4R3A* led to reduced occupancy of both Pol II and HYL1 at *MIR* genes, lower levels of pri-miRNAs, and fewer D-bodies compared with wild type. PP4R3A is a chromatin-associated protein that is present at the promoters of *MIR* genes and interacts with Pol II. One model is that PP4 recruits Pol II to *MIR* genes to promote their transcription, and at *MIR* loci, it dephosphorylates HYL1 to enable pri-miRNA processing (Su et al., 2017); hypophosphorylated HYL1 is active in pri-miRNA processing (Manavella et al., 2012). Alternatively, PP4 might dephosphorylate a chromatin protein to facilitate the access of both Pol II and hypophosphorylated HYL1 to chromatin.

The coordination of splicing and miRNA biogenesis has been well documented (Stepien et al., 2017). Pri-miRNAs may contain introns or may reside in introns of host genes, such that miRNA biogenesis may entail intron removal from pri-miRNAs, and microprocessor-mediated pri-miRNA cropping from introns of host genes may affect the splicing of host pre-mRNAs. However, in Arabidopsis, it is estimated that only half of the known pri-miRNAs contain introns (Szweykowska-Kulińska et al., 2013; Stepien et al., 2017). Yet, many splicing-related proteins have been found to affect miRNA biogenesis in general. For example, the nuclear cap binding complex, known to promote pre-mRNA splicing and polyadenylation, is required for pri-miRNA processing (Laubinger et al., 2008; Raczynska et al., 2014). The K-homology domain protein REGULATOR OF CBF GENE EXPRESSION3 interacts with the CPL phosphatases and promotes dephosphorylation of HYL1 in specific plant tissues to promote miRNA biogenesis. REGULATOR OF CBF GENE EXPRESSION3 and CPL1 also interact with the Arg-Ser (RS)-rich splicing factors RS40 and RS41 to promote intron splicing in many stress-related genes under salt stress (Chen et al., 2013; Karlsson et al., 2015). The Arabidopsis MAC is an ortholog of NineTeen Complex/Precursor mRNA processing19 Complex, which is well known for its function in RNA splicing in yeast and mammals (Chanarat and Sträßer, 2013). Intriguingly, studies of MAC subunits such as MAC3A, MAC3B, MAC7, PRL1, and PRL2 revealed that MAC not only functions in pre-mRNA splicing, but it also functions in miRNA biogenesis through an association with Pol II and/or the microprocessor (Zhang et al., 2013, 2014; Jia et al., 2017; Li et al., 2018). PP4R3A is similar to MAC in many respects, such as its association with Pol II and promotion of pri-miRNA processing, as well as the splicing of hundreds of pre-mRNAs. Our analyses showed that MAC and PP4 act on a small number of common introns and larger numbers of different introns to promote their splicing. These complexes both also act in miRNA biogenesis in general. We suspect that the ever-growing list of proteins that affect both miRNA biogenesis and RNA splicing does not necessarily imply that the two processes are linked, but rather, the two processes may involve common factors.

METHODS

Plant Materials and Growth Conditions

All Arabidopsis (*Arabidopsis thaliana*) plants used in this study are in the Columbia accession background and were grown under long photoperiod conditions (16-h light/8-h dark; white light; light intensity, 120 μmol m^{-2} s^{-1}) at 22°C. To assess the impact of temperature on the levels of HYL1, SE, and AGO1, 1-week-old seedlings were grown at 22°C and transferred to growth chambers at 16°C, 22°C, or 30°C for 1 more week. The T-DNA insertion mutants *pp4r3b-1* (SALK_022912), *pp4r3b-2* (SALK_138884), and *pp4r3a-2* (SAIL_33_H01; this allele is the same as *smek1-2*; Su et al., 2017) were obtained from the ABRC; *hyl1-2* (Han et al., 2004), *nrpb2-3* (Zheng et al., 2009), *cdc5-1* (Zhang et al., 2013), and *dcl1-20* (Li et al., 2016) were previously described. The *HYL1-YFP/pp4r3a-1*, *pMIR167a:GUS/pp4r3a-1*, and *pMIR172b:GUS/pp4r3a-1* lines were generated from crosses between *pp4r3a-1* and the transgenic lines *HYL1-YFP* (Fang and Spector, 2007), *pMIR167a:GUS* (Zhang et al., 2014), and *pMIR172b:GUS* (Zhang et al., 2013), respectively.

Mutagenesis and Screening

The *SUC2:amiR-SUL* transgenic lines were previously described (de Felippes et al., 2011). A stable line with a moderate leaf bleaching phenotype and one copy of a T-DNA insertion (designated as *amiR-SUL*) was used as the parental line for ethyl methanesulfonate mutagenesis. The *sup-e33* mutant was isolated based on its weaker leaf bleaching phenotype.

The method used for CRISPR/Cas9-mediated mutagenesis in the present study was reported previously (Yan et al., 2015). Genomic DNA was extracted from individual T1 or T2 transgenic plants, and the fragments flanking target sites were amplified with specific primer pairs and directly sequenced. The sequencing chromatograms were examined for exact patterns that indicate monoallelic or diallelic mutations.

DNA Constructs and Plant Transformation

To obtain the construct for the genetic complementation assay, a ~9-kb genomic DNA fragment containing the *PP4R3A* coding region and promoter was amplified from the Col genome and cloned into pENTR/D-TOPO (Invitrogen). The fragment was subsequently integrated into pGWB40 and pEG301, generating *pPP4R3A:PP4R3A-YFP* and *pPP4R3A:PP4R3A-HA*, respectively. For the *PP4R3A* and *PP4R3B* promoter-GUS constructs, the DNA fragment containing either the *PP4R3A* or *PP4R3B* promoter was PCR amplified and cloned into the destination vector pMDC162. For the *35S:PP4R3B-YFP* construct, the full-length CDS of *PP4R3B* without the stop codon was amplified and cloned into the pEG101 vector. CRISPR construction mainly involved two steps: first, the designed 20-bp guide RNA sequence targeting *PPX1* (GCCCATCAACTAGTTATGGA) or *PPX2* (GACCGTATAACTCTCATTAG) was cloned into the Bsa I-digested small guide RNA (sgRNA) scaffold where the sgRNA is driven by the *AtU6-26* promoter, and then the *AtU6-26:sgRNA* cassette was introduced into the binary vector *pYAO*(Yan et al., 2015)*:Cas9* cassette-containing pCambia 1300 where the *Cas9* gene is driven by the embryo-specific promoter of the *YAOZHE* (*YAO*) gene (Li et al., 2010).

The constructs were transferred into *Agrobacterium tumefaciens* strain GV3101 and introduced into plants by the floral dip method (Zhang et al., 2006). The primers used are listed in Supplemental Data Set 3.

GUS Staining and Microscopy

Plant tissues from homozygous transgenic lines were immersed in GUS staining buffer containing 50 mM sodium phosphate (pH 7.0), 0.5 mg/mL 5-Bromo-4-chloro-3-indolyl-β-D-glucuronic acid cyclohexylammonium salt (X-gluc), 0.1% Triton X-100, 2 mM potassium ferrocyanide, 2 mM potassium ferricyanide, and 10 mM EDTA and incubated at 37°C in the dark. The tissues were photographed under a stereomicroscope (Leica) after chlorophyll removal in 70% ethanol.

RT-qPCR and Small RNA Gel Blotting

Total RNAs were extracted from Arabidopsis tissues with TRIzol reagent (Medical Research Center) and treated with DNase I (Roche). First-strand complementary DNA was synthesized according to the manufacturer's instructions (Thermo Fisher Scientific). RT-qPCR was performed in the CFX96 Real-time System (Bio-Rad) using SYBR Green I Supermix (Bio-Rad). *UBQ5* served as an internal control. The procedure was previously described in detail (Jia et al., 2017). The primers are listed in Supplemental Data Set 3.

RNA gel blot analysis for small RNA detection was performed as described (Park et al., 2002). Total RNAs were extracted from 12-d-old seedlings. To detect miRNAs and tasiRNAs, 5′-end labeled ([γ-^{32}P] ATP) antisense DNA oligonucleotides were used as probes. Signals were quantified with ImageQuant 5.2 software and normalized to that of small nuclear RNA U6. The sequences of probes are shown in Supplemental Data Set 3.

Construction and Data Analysis of Small RNA-seq and RNA-seq Libraries

To construct the small RNA libraries, 50 μg total RNAs from 12-d-old seedlings were separated on a 15% urea-PAGE gel from which RNAs in the desired size range (10-40 nucleotide) were recovered. Small RNA libraries were constructed using a New England BioLabs (NEB) Next Multiplex Small RNA Library Prep kit (NEB, E7300S) following the manufacturer's instructions. Before RNA-seq library construction, poly(A)$^+$ RNAs were isolated from 5 μg total RNAs from 12-d-old seedlings using a Magnetic mRNA Isolation kit (NEB, S1550S). RNA-seq libraries were constructed using a NEBNext mRNA Library Prep Reagent Set for Illumina (NEB, E6110). Both small RNA and RNA-seq libraries were pooled and sequenced on the Illumina HiSeq 2500 platform. The data analysis of small RNA seq and RNA-seq libraries was described (Jia et al., 2017). To analyze pri-miRNA levels, 325 pri-miRNAs annotated in Araport11 were interrogated, and those that were represented by reads of FPKM>2 were retained. Some pri-miRNA loci overlapped with protein-coding genes, whereas others did not (Lepe-Soltero et al., 2017); those not overlapping with protein-coding genes were separately analyzed. The 131 miRNA-target pairs validated from previous degradome or rapid-amplification of complementary DNA ends (RACE) experiments (Ma et al., 2018) were included in the analysis of the expression of miRNA target genes. The analysis of splicing defects was performed using Araport11 intron annotation and a previously developed pipeline known as SQUID (https://github.com/Xinglab/SQUID). In brief, the level of intron retention is calculated for each intron as the percentage of intron reads $(intron\text{ - }exon\ junction\ reads/[intron\text{ - }exon\ junction\ reads + exon\text{-}exon\ junction\ reads])$.

Co-immunoprecipitation and Protein Gel Blot Analysis

Approximately 0.5 g of tissue from 12-d-old F1 plants from a cross between *PP4R3A-YFP* and *RPB1-MYC* transgenic lines was ground in liquid nitrogen and homogenized in IP buffer containing 20 mM Tris·HCl (pH 7.5), 150 mM NaCl, 4 mM $MgCl_2$, 75 μM $ZnCl_2$, 0.1% Triton X-100, 1% glycerol, and EDTA-free protease inhibitor mixture (Roche). Cleared protein extracts were immunoprecipitated using anti-c-MYC Affinity Gel (Sigma, E6654) or GFP-Trap (ChromoTek, gtm-10). The bound proteins were washed twice with IP buffer and separated by SDS-PAGE. Protein gel blot analysis was performed using anti-MYC (1:1000, Millipore, 05-724) or GFP (1:1000, Roche, 11814460001) antibodies.

To determine protein levels, total cellular proteins from 12-d-old seedlings were resolved by SDS-PAGE, transferred to nitrocellulose membranes, and detected using antibodies against RPB1 (1:1000, Agrisera, AS111804), RPB2 (1:1000, Abcan, ab10338), HYL1 (1:2000, Agrisera, AS06136), AGO1 (1:2000, Agrisera, AS09527), AGO2 (1:2000, Agrisera, AS132682), and SE (1:1000, Agrisera, AS09532A).

Affinity Purification and Mass Spectrometric Analysis

Approximately 2 g of tissue from 12-d-old *PP4R3A-YFP* and *PP4R3A-HA* transgenic T3 plants, or Col plants as a negative control, were ground in liquid nitrogen. The powder was re-suspended in 10 mL of lysis buffer (50 mM Tris [pH 7.6], 150 mM NaCl, 5 mM $MgCl_2$, 1% glycerol, 0.1% Nonidet P-40, 0.5 mM DTT, 1 mM PMSF, and protease inhibitor cocktail) and incubated on a rotator for 10 min at 4°C. The slurry was filtered through four layers of Miracloth and centrifuged at 13,000*g* for 15 min at 4°C. Before immunoprecipitation, the supernatant was incubated with 100 μL of Dynabeads (Invitrogen, 10002D) for 2 h at 4°C. The pre-cleared supernatant was immunoprecipitated using GFP-Trap (ChromoTek, gtm-10) or anti-HA magnetic beads (88836, Pierce) according to the manufacturer's instructions. After incubation, the anti-GFP or anti-HA beads were washed three times with lysis buffer. The IP samples were resolved by SDS-PAGE and subjected to mass spectrometry as described (Sleat et al., 2006; Deng et al., 2016).

Extraction of Chromatin-Associated Proteins

Twelve-day-old seedlings were subjected to nuclear-cytoplasmic fractionation as previously described (Wang et al., 2011). The nuclei pellet was re-suspended in low-salt buffer (10 mM Tris-HCl [pH 7.4], 0.2 mM $MgCl_2$, and 1% Triton-X 100) supplemented with protease inhibitor cocktail (Roche), incubated on a rotator at 4°C for 30 min, and centrifuged at 6,500*g* for 10 min at 4°C. The chromatin pellet was washed twice with 5 volumes of

no-salt buffer (3 mM EDTA and 0.2 mM EGTA), re-suspended in 2-5 volumes of 0.2 N HCl, and incubated on a rotator at 4°C for 4 h. The solution was centrifuged at 14,000 rpm for 10 min at 4°C, and the supernatant (consisting of acid-soluble proteins from the chromatin fraction) was collected and neutralized with the same volume of 1M Tris-HCl (pH 8.0). GAPDH (Santa Cruz, sc-47724) and histone H3 (Abcam, ab10799) serve as the cytoplasmic and the nuclear marker, respectively.

ChIP

The ChIP assays of PP4R3A, Pol II, and HYL1 were performed as described previously (Yamaguchi et al., 2014). For ChIP of HYL1, 12-d-old Col and *pp4r3a-1* seedlings were processed and anti-HYL1 antibodies (Agrisera, AS06136) were used for immunoprecipitation; for PP4R3A, 12-d-old seedlings harboring *PP4R3A:PP4R3A-HA* and the negative control (wild type) were processed, and HA-probe (Santa Cruz, sc-7392) was used to pull down the protein–DNA complexes. Transgenic lines harboring isogenic *RPB1-MYC* in the Col and *pp4r3a-1* backgrounds were used for Pol II ChIP. Quantitative PCR was performed using immunoprecipitated DNA samples; relative enrichment was calculated by normalizing the amount of ChIP-ed DNA to the corresponding amount in the input. The primers used are listed in Supplemental Data Set 3.

Accession Numbers

Sequence data from this article can be found in the Arabidopsis Genome Initiative or GenBank/EMBL databases under the following accession numbers: *PP4R3A* (AT3G06670), *PP4R3B* (AT5G49370, AT5G49380, AT5G49390), *PP4R2L* (AT5G17070), *PPX1* (AT4G26720), *PPX2* (AT5G55260), *SUL* (AT4G18480), *SQUAMOSA PROMOTER BINDING PROTEIN-LIKE5* (AT3G15270), *PHABULOSA* (AT2G34710), *PHAVOLUTA* (AT1G30490), *REV* (AT5G60690), *MYB33* (AT5G06100), *AGO1* (AT1G48410), *AUXIN RESPONSE FACTOR8* (AT5G37020), *AGO2* (AT1G31280), *SE* (AT2G27100), *DCL1* (AT1G01040), *HYL1* (AT1G09700), *CDC5* (AT1G09770), *RPB1* (AT4G35800), *RPB2/NRPB2* (AT4G21710), *CPL1* (AT4G21670), *HEN1* (AT4G20910), *MOS2* (AT1G33520), *NOT2A* (AT1G07705), *NOT2B* (AT5G18230), *PRL1* (AT4G15900), *DDL* (AT3G20550), *TGH* (AT5G23080), *CPB20* (AT5G44200), *CPB80* (AT2G13540), and *HST* (AT3G05040). The small RNA- and RNA-seq data were deposited in the Gene Expression Omnibus database under accession number GSE121456.

Supplemental Data

Supplemental Figure 1. Phenotypes of *sup-e33* mutant plants.

Supplemental Figure 2. *PP4R3A* expression in wide type and two *pp44r3* mutants, as revealed by RNA-seq.

Supplemental Figure 3. Mutations in *PP4R3A* lead to shortened roots.

Supplemental Figure 4. Hierarchical clustering analysis showing the degree of similarity among the sRNA-seq libraries.

Supplemental Figure 5. Tissue-specific expression patterns of *pPP4R3A:GUS* and *pPP4R3B:GUS.*

Supplemental Figure 6. The *35S:PP4R3B* transgene does not rescue the phenotypes of *pp4r3a-1.*

Supplemental Figure 7. Phenotypes of *pp4r3a-1* rescued with YFP- or HA-tagged PP4R3A transgenes.

Supplemental Figure 8. Composition of PP4, and mutants of PP4 catalytic subunit genes.

Supplemental Figure 9. Mutations in *PP4R3A* do not affect the expression of genes involved in miRNA biogenesis.

Supplemental Figure 10. Accumulation of endogenous miRNAs in microprocessor mutants and in double mutants between *sup-e33* and microprocessor mutants.

Supplemental Figure 11. PP4R3A does not associate with the microprocessor subunits HYL1 and SE in vivo, and HYL1 is not required for the occupancy of PP4R3A at *MIR* promoters.

Supplemental Figure 12. RNA-seq of wild type and two *pp4r3a* mutants reveals global changes of the expression of miRNA targets and pri-miRNAs in the mutants.

Supplemental Figure 13. RNA-seq reveals changes in gene expression and defects in pre-mRNA splicing in the mutants.

Supplemental Figure 14. Features of retained introns and genes with intron retention in two *pp4r3a* alleles.

Supplemental Data Set 1. Levels of miRNAs in wild type (Col), *pp4r3a-1*, and *pp4r3-2*, as determined by small RNA sequencing.

Supplemental Data Set 2. List of proteins identified by IP-MS.

Supplemental Data Set 3. Sequences of primers and probes used in this study.

ACKNOWLEDGMENTS

We are grateful to Dr. B. Yu (University of Nebraska–Lincoln) for sharing Arabidopsis mutants and transgenic lines. We thank Dr. H. Zheng (Rutgers University) for technical support in mass spectrometry analysis. This project was funded by Guangdong Innovation Research Team Fund (2014ZT05S078), National Science Foundation of China (91740202, 31571332), National Institutes of Health (GM129373) and China Postdoctoral Science Foundation (2017M612717).

AUTHOR CONTRIBUTIONS

S.W., B.M., and X.C. conceived the project; S.W., L.Q., L.L., and Y.Z. designed and performed the experiments; S.L., C.Y., L.G., L.Z., and Y.Q. analyzed the data; S.W. and X.C. wrote the manuscript.

Received July 24, 2018; revised November 28, 2018; accepted January 16, 2019; published January 23, 2019.

REFERENCES

Achkar, N.P., et al. (2018). A quick HYL1-dependent reactivation of microRNA production is required for a proper developmental response after extended periods of light deprivation. Dev. Cell **46:** 236–247.e6.

Ahn, C.S., Han, J.A., Lee, H.S., Lee, S., and Pai, H.S. (2011). The PP2A regulatory subunit Tap46, a component of the TOR signaling pathway, modulates growth and metabolism in plants. Plant Cell **23:** 185–209.

Allen, E., Xie, Z., Gustafson, A.M., and Carrington, J.C. (2005). microRNA-directed phasing during trans-acting siRNA biogenesis in plants. Cell **121:** 207–221.

Armenta-Medina, A., Lepe-Soltero, D., Xiang, D., Datla, R., Abreu-Goodger, C., and Gillmor, C.S. (2017). *Arabidopsis thaliana*

miRNAs promote embryo pattern formation beginning in the zygote. Dev. Biol. **431:** 145–151.

Ballarino, M., Pagano, F., Girardi, E., Morlando, M., Cacchiarelli, D., Marchioni, M., Proudfoot, N.J., and Bozzoni, I. (2009). Coupled RNA processing and transcription of intergenic primary microRNAs. Mol. Cell. Biol. **29:** 5632–5638.

Ben Chaabane, S., Liu, R., Chinnusamy, V., Kwon, Y., Park, J.H., Kim, S.Y., Zhu, J.K., Yang, S.W., and Lee, B.H. (2013). STA1, an *Arabidopsis* pre-mRNA processing factor 6 homolog, is a new player involved in miRNA biogenesis. Nucleic Acids Res. **41:** 1984–1997.

Bielewicz, D., Kalak, M., Kalyna, M., Windels, D., Barta, A., Vazquez, F., Szweykowska-Kulinska, Z., and Jarmolowski, A. (2013). Introns of plant pri-miRNAs enhance miRNA biogenesis. EMBO Rep. **14:** 622–628.

Chanarat, S., and Sträßer, K. (2013). Splicing and beyond: The many faces of the Prp19 complex. Biochim. Biophys. Acta **1833:** 2126–2134.

Chen, T., Cui, P., Chen, H., Ali, S., Zhang, S., and Xiong, L. (2013). A KH-domain RNA-binding protein interacts with FIERY2/CTD phosphatase-like 1 and splicing factors and is important for pre-mRNA splicing in *Arabidopsis.* PLoS Genet. **9:** e1003875.

Chen, T., Cui, P., and Xiong, L. (2015). The RNA-binding protein HOS5 and serine/arginine-rich proteins RS40 and RS41 participate in miRNA biogenesis in *Arabidopsis.* Nucleic Acids Res. **43:** 8283–8298.

Cho, S.K., Ben Chaabane, S., Shah, P., Poulsen, C.P., and Yang, S. W. (2014). COP1 E3 ligase protects HYL1 to retain microRNA biogenesis. Nat. Commun. **5:** 5867.

Cho, S.K., Ryu, M.Y., Shah, P., Poulsen, C.P., and Yang, S.W. (2016). Post-translational regulation of miRNA pathway components, AGO1 and HYL1, in plants. Mol. Cells **39:** 581–586.

Chowdhury, D., Xu, X., Zhong, X., Ahmed, F., Zhong, J., Liao, J., Dykxhoorn, D.M., Weinstock, D.M., Pfeifer, G.P., and Lieberman, J. (2008). A PP4-phosphatase complex dephosphorylates gamma-H2AX generated during DNA replication. Mol. Cell **31:** 33–46.

Cohen, P.T., Philp, A., and Vázquez-Martin, C. (2005). Protein phosphatase 4--from obscurity to vital functions. FEBS Lett. **579:** 3278–3286.

de Felippes, F.F., Ott, F., and Weigel, D. (2011). Comparative analysis of non-autonomous effects of tasiRNAs and miRNAs in *Arabidopsis thaliana.* Nucleic Acids Res. **39:** 2880–2889.

Deng, X., Lu, T., Wang, L., Gu, L., Sun, J., Kong, X., Liu, C., and Cao, X. (2016). Recruitment of the NineTeen Complex to the activated spliceosome requires AtPRMT5. Proc. Natl. Acad. Sci. USA **113:** 5447–5452.

Dong, Z., Han, M.H., and Fedoroff, N. (2008). The RNA-binding proteins HYL1 and SE promote accurate in vitro processing of pri-miRNA by DCL1. Proc. Natl. Acad. Sci. USA **105:** 9970–9975.

Eamens, A.L., Smith, N.A., Curtin, S.J., Wang, M.B., and Waterhouse, P.M. (2009). The *Arabidopsis thaliana* double-stranded RNA binding protein DRB1 directs guide strand selection from microRNA duplexes. RNA **15:** 2219–2235.

Fang, Y., and Spector, D.L. (2007). Identification of nuclear dicing bodies containing proteins for microRNA biogenesis in living *Arabidopsis* plants. Curr. Biol. **17:** 818–823.

Fang, X., Cui, Y., Li, Y., and Qi, Y. (2015). Transcription and processing of primary microRNAs are coupled by Elongator complex in *Arabidopsis.* Nat. Plants **1:** 15075.

Fei, Q., Xia, R., and Meyers, B.C. (2013). Phased, secondary, small interfering RNAs in posttranscriptional regulatory networks. Plant Cell **25:** 2400–2415.

Gingras, A.C., Caballero, M., Zarske, M., Sanchez, A., Hazbun, T.R., Fields, S., Sonenberg, N., Hafen, E., Raught, B., and Aebersold, R. (2005). A novel, evolutionarily conserved protein phosphatase complex involved in cisplatin sensitivity. Mol. Cell. Proteomics **4:** 1725–1740.

Golden, T.A., Schauer, S.E., Lang, J.D., Pien, S., Mushegian, A.R., Grossniklaus, U., Meinke, D.W., and Ray, A. (2002). SHORT INTEGUMENTS1/SUSPENSOR1/CARPEL FACTORY, a Dicer homolog, is a maternal effect gene required for embryo development in *Arabidopsis.* Plant Physiol. **130:** 808–822.

Grigg, S.P., Canales, C., Hay, A., and Tsiantis, M. (2005). SERRATE coordinates shoot meristem function and leaf axial patterning in *Arabidopsis.* Nature **437:** 1022–1026.

Han, M.H., Goud, S., Song, L., and Fedoroff, N. (2004). The *Arabidopsis* double-stranded RNA-binding protein HYL1 plays a role in microRNA-mediated gene regulation. Proc. Natl. Acad. Sci. USA **101:** 1093–1098.

Harris, D.M., Myrick, T.L., and Rundle, S.J. (1999). The *Arabidopsis* homolog of yeast TAP42 and mammalian alpha4 binds to the catalytic subunit of protein phosphatase 2A and is induced by chilling. Plant Physiol. **121:** 609–617.

Hastie, C.J., Vázquez-Martin, C., Philp, A., Stark, M.J., and Cohen, P.T. (2006). The *Saccharomyces cerevisiae* orthologue of the human protein phosphatase 4 core regulatory subunit R2 confers resistance to the anticancer drug cisplatin. FEBS J. **273:** 3322–3334.

Jia, T., Zhang, B., You, C., Zhang, Y., Zeng, L., Li, S., Johnson, K.C. M., Yu, B., Li, X., and Chen, X. (2017). The *Arabidopsis* MOS4-associated complex promotes microRNA biogenesis and precursor messenger RNA splicing. Plant Cell **29:** 2626–2643.

Karlsson, P., Christie, M.D., Seymour, D.K., Wang, H., Wang, X., Hagmann, J., Kulcheski, F., and Manavella, P.A. (2015). KH domain protein RCF3 is a tissue-biased regulator of the plant miRNA biogenesis cofactor HYL1. Proc. Natl. Acad. Sci. USA **112:** 14096–14101.

Kataya, A.R.A., Creighton, M.T., Napitupulu, T.P., Sætre, C., Heidari, B., Ruoff, P., and Lillo, C. (2017). PLATINUM SENSITIVE 2 LIKE impacts growth, root morphology, seed set, and stress responses. PLoS One **12:** e0180478.

Kim, Y.J., Zheng, B., Yu, Y., Won, S.Y., Mo, B., and Chen, X. (2011). The role of Mediator in small and long noncoding RNA production in *Arabidopsis thaliana.* EMBO J. **30:** 814–822.

Komiya, R. (2017). Biogenesis of diverse plant phasiRNAs involves an miRNA-trigger and Dicer-processing. J. Plant Res. **130:** 17–23.

Kurihara, Y., and Watanabe, Y. (2004). *Arabidopsis* micro-RNA biogenesis through Dicer-like 1 protein functions. Proc. Natl. Acad. Sci. USA **101:** 12753–12758.

Laubinger, S., Sachsenberg, T., Zeller, G., Busch, W., Lohmann, J. U., Rätsch, G., and Weigel, D. (2008). Dual roles of the nuclear cap-binding complex and SERRATE in pre-mRNA splicing and microRNA processing in *Arabidopsis thaliana.* Proc. Natl. Acad. Sci. USA **105:** 8795–8800.

Lee, D.H., Pan, Y., Kanner, S., Sung, P., Borowiec, J.A., and Chowdhury, D. (2010). A PP4 phosphatase complex dephosphorylates RPA2 to facilitate DNA repair via homologous recombination. Nat. Struct. Mol. Biol. **17:** 365–372.

Lee, D.H., Goodarzi, A.A., Adelmant, G.O., Pan, Y., Jeggo, P.A., Marto, J.A., and Chowdhury, D. (2012). Phosphoproteomic analysis reveals that PP4 dephosphorylates KAP-1 impacting the DNA damage response. EMBO J. **31:** 2403–2415.

Lepe-Soltero, D., Armenta-Medina, A., Xiang, D., Datla, R., Gillmor, C.S., and Abreu-Goodger, C. (2017). Annotating and quantifying pri-miRNA transcripts using RNA-Seq data of wild type

and *serrate-1* globular stage embryos of *Arabidopsis thaliana.* Data Brief **15:** 642–647.

Li, H.J., Liu, N.Y., Shi, D.Q., Liu, J., and Yang, W.C. (2010). YAO is a nucleolar WD40-repeat protein critical for embryogenesis and gametogenesis in Arabidopsis. BMC Plant Biol. **10:** 169. 20699009

Li, S., Le, B., Ma, X., Li, S., You, C., Yu, Y., Zhang, B., Liu, L., Gao, L., Shi, T., Zhao, Y., and Mo, B., et al. (2016). Biogenesis of phased siRNAs on membrane-bound polysomes in *Arabidopsis.* eLife **5:** e22750.

Li, S., Liu, K., Zhou, B., Li, M., Zhang, S., Zeng, L., Zhang, C., and Yu, B. (2018). MAC3A and MAC3B, two core subunits of the MOS4-associated complex, positively influence miRNA biogenesis. Plant Cell **30:** 481–494.

Lillo, C., Kataya, A.R., Heidari, B., Creighton, M.T., Nemie-Feyissa, D., Ginbot, Z., and Jonassen, E.M. (2014). Protein phosphatases PP2A, PP4 and PP6: Mediators and regulators in development and responses to environmental cues. Plant Cell Environ. **37:** 2631–2648.

Liu, J., Xu, L., Zhong, J., Liao, J., Li, J., and Xu, X. (2012). Protein phosphatase PP4 is involved in NHEJ-mediated repair of DNA double-strand breaks. Cell Cycle **11:** 2643–2649.

Ma, X., Liu, C., Gu, L., Mo, B., Cao, X., and Chen, X. (2018). TarHunter, a tool for predicting conserved microRNA targets and target mimics in plants. Bioinformatics **34:** 1574–1576.

Manavella, P.A., Hagmann, J., Ott, F., Laubinger, S., Franz, M., Macek, B., and Weigel, D. (2012). Fast-forward genetics identifies plant CPL phosphatases as regulators of miRNA processing factor HYL1. Cell **151:** 859–870.

Moorhead, G.B., De Wever, V., Templeton, G., and Kerk, D. (2009). Evolution of protein phosphatases in plants and animals. Biochem. J. **417:** 401–409.

Morlando, M., Ballarino, M., Gromak, N., Pagano, F., Bozzoni, I., and Proudfoot, N.J. (2008). Primary microRNA transcripts are processed co-transcriptionally. Nat. Struct. Mol. Biol. **15:** 902–909.

Park, W., Li, J., Song, R., Messing, J., and Chen, X. (2002). CARPEL FACTORY, a Dicer homolog, and HEN1, a novel protein, act in microRNA metabolism in *Arabidopsis thaliana.* Curr. Biol. **12:** 1484–1495.

Raczynska, K.D., Stepien, A., Kierzkowski, D., Kalak, M., Bajczyk, M., McNicol, J., Simpson, C.G., Szweykowska-Kulinska, Z., Brown, J.W., and Jarmolowski, A. (2014). The SERRATE protein is involved in alternative splicing in *Arabidopsis thaliana.* Nucleic Acids Res. **42:** 1224–1244.

Raghuram, B., Sheikh, A.H., Rustagi, Y., and Sinha, A.K. (2015). MicroRNA biogenesis factor DRB1 is a phosphorylation target of mitogen activated protein kinase MPK3 in both rice and *Arabidopsis.* FEBS J. **282:** 521–536.

Rogers, K., and Chen, X. (2013). Biogenesis, turnover, and mode of action of plant microRNAs. Plant Cell **25:** 2383–2399.

Sleat, D.E., Zheng, H., Qian, M., and Lobel, P. (2006). Identification of sites of mannose 6-phosphorylation on lysosomal proteins. Mol. Cell. Proteomics **5:** 686–701.

Stepien, A., Knop, K., Dolata, J., Taube, M., Bajczyk, M., Barciszewska-Pacak, M., Pacak, A., Jarmolowski, A., and Szweykowska-Kulinska, Z. (2017). Posttranscriptional coordination of splicing and miRNA biogenesis in plants. Wiley Interdiscip. Rev. RNA **8:** e1403.

Su, C., Li, Z., Cheng, J., Li, L., Zhong, S., Liu, L., Zheng, Y., and Zheng, B. (2017). The protein phosphatase 4 and SMEK1 complex dephosphorylates HYL1 to promote miRNA biogenesis by antagonizing the MAPK cascade in *Arabidopsis.* Dev. Cell **41:** 527–539.e5.

Szweykowska-Kulińska, Z., Jarmolowski, A., and Vazquez, F. (2013). The crosstalk between plant microRNA biogenesis factors and the spliceosome. Plant Signal. Behav. **8:** e26955.

Wang, L., Song, X., Gu, L., Li, X., Cao, S., Chu, C., Cui, X., Chen, X., and Cao, X. (2013). NOT2 proteins promote polymerase II-dependent transcription and interact with multiple MicroRNA biogenesis factors in *Arabidopsis.* Plant Cell **25:** 715–727.

Wang, W., Ye, R., Xin, Y., Fang, X., Li, C., Shi, H., Zhou, X., and Qi, Y. (2011). An importin β protein negatively regulates MicroRNA activity in *Arabidopsis.* Plant Cell **23:** 3565–3576.

Xie, Z., Allen, E., Fahlgren, N., Calamar, A., Givan, S.A., and Carrington, J.C. (2005). Expression of *Arabidopsis* MIRNA genes. Plant Physiol. **138:** 2145–2154.

Yamaguchi, N., Winter, C.M., Wu, M.F., Kwon, C.S., William, D.A., and Wagner, D. (2014). PROTOCOLS: Chromatin immunoprecipitation from *Arabidopsis* tissues. The Arabidopsis Book **12:** e0170.

Yan, J., et al. (2017). The SnRK2 kinases modulate miRNA accumulation in *Arabidopsis.* PLoS Genet. **13:** e1006753.

Yan, L., Wei, S., Wu, Y., Hu, R., Li, H., Yang, W., and Xie, Q. (2015). High efficiency genome editing in *Arabidopsis* using Yao promoter-driven CRISPR/Cas9 system. Mol. Plant **8:** 1820–1823.

Yan, L., Wei, S., Wu, Y., Hu, R., Li, H., Yang, W., and Xie, Q. (2015). High-Efficiency Genome Editing in Arabidopsis Using YAO Promoter-Driven CRISPR/Cas9 System. Mol. Plant **8:** 1820–1823. 26524930

Zhan, X., Wang, B., Li, H., Liu, R., Kalia, R.K., Zhu, J.K., and Chinnusamy, V. (2012). *Arabidopsis* proline-rich protein important for development and abiotic stress tolerance is involved in microRNA biogenesis. Proc. Natl. Acad. Sci. USA **109:** 18198–18203.

Zhang, S., Xie, M., Ren, G., and Yu, B. (2013). CDC5, a DNA binding protein, positively regulates posttranscriptional processing and/or transcription of primary microRNA transcripts. Proc. Natl. Acad. Sci. USA **110:** 17588–17593.

Zhang, S., Liu, Y., and Yu, B. (2014). PRL1, an RNA-binding protein, positively regulates the accumulation of miRNAs and siRNAs in *Arabidopsis.* PLoS Genet. **10:** e1004841.

Zhang, X., Henriques, R., Lin, S.S., Niu, Q.W., and Chua, N.H. (2006). *Agrobacterium*-mediated transformation of *Arabidopsis thaliana* using the floral dip method. Nat. Protoc. **1:** 641–646.

Zheng, B., Wang, Z., Li, S., Yu, B., Liu, J.Y., and Chen, X. (2009). Intergenic transcription by RNA polymerase II coordinates Pol IV and Pol V in siRNA-directed transcriptional gene silencing in *Arabidopsis.* Genes Dev. **23:** 2850–2860.